

Extension of the synchrotron radiation of electrons to very high energies in clumpy environments

DMITRY KHANGULYAN,¹ FELIX AHARONIAN,^{2,3} CARLO ROMOLI,⁴ AND ANDREW TAYLOR⁵

¹*Department of Physics, Rikkyo University, Nishi-Ikebukuro 3-34-1, Toshima-ku, Tokyo 171-8501, Japan*

²*Dublin Institute for Advanced Studies, School of Cosmic Physics, 31 Fitzwilliam Place, Dublin 2, Ireland*

³*Max-Planck-Institut für Kernphysik, Saupfercheckweg 1, 69117 Heidelberg, Germany*

⁴*Max-Planck-Institut für Kernphysik, Saupfercheckweg 1, 69117 Heidelberg, Germany*

⁵*DESY, D-15738 Zeuthen, Germany*

(Received January 15, 2021; Revised January 10, 2019; Accepted May 12, 2021)

Submitted to ApJ

ABSTRACT

The synchrotron cooling of relativistic electrons is one of the most effective radiation mechanisms in astrophysics. It not only accompanies the process of particle acceleration but also has feedback on the formation of the energy distribution of the parent electrons. The radiative cooling time of electrons decreases with energy as $t_{\text{SYN}} \propto 1/E$; correspondingly the overall radiation efficiency increases with energy. On the other hand, this effect strictly limits the maximum energy of individual photons. Even in the so-called extreme accelerators, where the acceleration proceeds at the highest possible rate, $t_{\text{ACC}}^{-1} = eBc/E$, allowed in an ideal magnetohydrodynamic plasma, the synchrotron radiation cannot extend well beyond the characteristic energy determined by the electron mass and the fine-structure constant: $h\nu^{\text{MAX}} \sim m_e c^2 / \alpha \sim 70 \text{ MeV}$. In this paper, we propose a model in which the formation of synchrotron radiation takes place in compact magnetic blobs located inside the particle accelerator and develop a formalism for calculations of synchrotron radiation emerging from such systems. We demonstrate that for certain combinations of parameters characterizing the accelerator and the magnetic blobs, the synchrotron radiation can extend beyond this limit by a several orders of magnitude. This scenario requires a weak magnetization of the particle accelerator, and an efficient conversion of gas internal energy into magnetic energy in sufficiently small blobs. The required size of the blobs is constrained by the magnetic mirroring effect, that can prevent particle penetration into the regions of strong magnetic field under certain conditions.

Keywords: editorials, notices — miscellaneous — catalogs — surveys

1. INTRODUCTION

Acceleration of non-thermal particles in various astrophysical environments requires the presence of electric field. If high-energy particles are accelerated in a region with a typical magnetic field, B_0 , then the time, required for the particle to gain energy E , is $t_{\text{ACC}} = \eta E / (eB_0 c)$. Here, η is a dimensionless parameter, namely the ratio of the magnetic to the accelerating electric field, $\eta = B_0 / \mathcal{E}_0$. If the acceleration proceeds in a magnetohydrodynamic (MHD) flow, then $\mathcal{E}_0 < B_0$ and the acceleration efficiency is constrained by $\eta > 1$. The acceleration is efficient only in the energy range where the acceleration time is shorter than the cooling time. For the case where synchrotron losses dominate, the cooling time is $t_{\text{SYN}} = 6\pi m_e^2 c^3 / (\sigma_T B_0^2 E)$ (here m_e , c , and σ_T are electron mass, speed of light, and Thomson cross-section, respectively). The electrons are subsequently accelerated up to a maximum energy $E_e^{\text{MAX}} = \sqrt{6\pi e m_e^2 c^4 / (\sigma_T \eta B_0)}$. Correspondingly, the electrons which achieve this energy, produce synchrotron photons of energy $h\nu^{\text{MAX}} \approx m_e c^2 / (\alpha \eta) \approx 70 \eta^{-1} \text{ MeV}$ (Guilbert et al. 1983, here α is the fine-structure constant). We note that this energy

corresponds to the spectral maximum of synchrotron emission produced by an electron of energy E_e^{MAX} moving in a magnetic field B_0 perpendicular to the velocity of the electron. Various factors can shift the exact position of the synchrotron maximum (for example, particle velocity – magnetic field pitch angle; turbulent dispersion of magnetic field strength; energy distribution of emitting particles; etc). However, the impact of these factors is expected to be small (see, e.g., [Derishev & Aharonian 2019](#), for the comparison of the spectra averaged over pitch angle and turbulent distribution of magnetic field strength). A much more important factor is that this limit was obtained under the assumption of the perfect operation of the acceleration process, which is likely not achievable in real astrophysical accelerators. Thus, we adopt the above obtained energy as an energy that limits the extension of the synchrotron component (which is sometimes referred in literature as *synchrotron burnoff limit*, see, e.g., [de Jager et al. 1996](#)). Finally, we note that the maxim of the spectral energy distribution (SED) appears at higher energies, namely for the same underlying assumptions at $\approx 300\eta^{-1}$ MeV.

There are several ways to alleviate this constraint on the cutoff energy of synchrotron component. Examples of a bypass are the inclusion of relativistic motion of the production site, acceleration with efficiencies exceeding the ideal MHD threshold ($\eta < 1$), synchrotron emission of secondary electron positron pairs, synchrotron emission by particles heavier than electrons (muons and protons), and special regimes of emission (for example, in small-scale turbulent magnetic field). We discuss these approaches in Sec. 2 in more detail. In this paper, we explore a new scenario for boosting the energy range of the synchrotron radiation utilising the structure of the ambient magnetic field in the acceleration region. The principle behind our proposed scheme is the separation of the region of the electron acceleration and the region(s) of effective synchrotron radiation. More specifically, we consider a scenario in which the acceleration region contains a large number of compact magnetic field condensations (blobs), whose collective volume filling factor is small. Provided that the particle-blob collision time is long compared to the acceleration time, these blobs have only a minor impact on the acceleration process. On the other hand, high-energy particles that eventually collide with these blob regions give rise to a synchrotron radiation component which can extend well beyond 100 MeV. Throughout the discussion, we do not specify the acceleration mechanism, as well as the nature of the compact magnetic condensations, but focus on the propagation and radiation of the accelerated electrons colliding with the dense magnetic blobs. A high degree of inhomogeneity of magnetic plasma is favored by numerical simulations of shocks, magnetic reconnection, and turbulence. The general consideration of the suggested scenario is therefore potentially relevant for a number of astrophysical systems.

2. MAGNETOBREMSSTRAHLUNG FEEDBACK ON PARTICLE SPECTRUM

The synchrotron burnoff turnover is caused by the feedback of synchrotron cooling on particle acceleration in ideal MHD plasma and should be applied in the plasma co-moving reference frame. In the most simple setup, where the magnetic field is homogeneous and perpendicular to the particle velocity, the cutoff should appear at $h\nu^{\text{MAX}} \sim 70\mathcal{D}m/(m_e\eta)$ MeV, where m and \mathcal{D} are mass of the emitting particle and the Doppler boosting factor, respectively. The Doppler boosting effect, which accounts for relativistic motion of the production site, can be sufficient to explain, in a framework of electron synchrotron scenario, bright Crab GeV flares, whose SED peaks at a few hundred MeV, $h\nu^{\text{MAX}} \lesssim 400$ MeV. However extension of the synchrotron component to the very high energy (VHE) regime requires an extremely high boosting factors $\mathcal{D} \sim \mathcal{O}(10^3)$. Such fast outflows are not expected in astrophysical objects unless one considers production of the emission in pulsar winds, whose bulk Lorentz factor can be very high, $\mathcal{D} \sim 10^6$. These winds originate in a very compact region, comparable in size to the pulsar magnetosphere, and almost unavoidably undergo strong adiabatic cooling due to their expansion. As a result, the temperature of the wind electrons (i.e., their energy in the co-moving frame) is expected to be very low, resulting in a strong suppression of the synchrotron emission. If some acceleration process, even with a modest efficiency, $\eta < 10^3$, operates in a pulsar wind, then the synchrotron emission produced there could be boosted into the VHE regime.

Another obvious way to generate synchrotron emission in the VHE domain is to consider higher-mass particles. For example, protons, whose mass is $\approx 2000m_e$, in an extreme accelerator, $\eta \sim 1$, produce a synchrotron component that reaches the VHE domain. A modest Doppler boosting, $\mathcal{D} \sim 30$, can relax the requirement for acceleration efficiency or extend the spectrum to multi-TeV energies. The high cutoff energy of proton synchrotron emission comes at a price of very large energy of emitting particles. The energy of particles that reach the synchrotron cooling limit scales as m^2 , thus proton synchrotron scenarios require a very strong magnetic field of $B \geq 100$ G needed to confine the ultra-high energy protons ([Aharonian 2000](#)).

Variations in other underlining assumptions may also change the position of the burnoff limit. For example, if a particle is on a trajectory closely following a bent magnetic field line then energy losses of the particle and its peak emitting frequency do not depend on the strength of the magnetic field but rather on its curvature radius. This emission mechanism is dubbed in literature as *curvature radiation*, and it is feasible that curvature radiation peaks above the synchrotron burnoff limit. Acceleration of particles for efficient emission via curvature radiation requires the presence of electric field directed along the magnetic field. This implies a violation of the ideal MHD conditions at least in certain regions of the source (in so-called *gaps*). Alternatively, one can consider the curvature radiation produced by secondary electrons, e.g., generated in pulsar magnetosphere by photon magnetic absorption. In this case the initial momentum of secondary particles is not necessary directed along the magnetic field, so the bulk of particle energy is emitted via the synchrotron channel. The “100 MeV” limit does not concern the synchrotron radiation produced by secondary electrons independently on the specific mechanism of their generation. For example, under suitable condition the products of interactions of primary protons with the surrounding gas or radiation fields can generate a synchrotron component that extends beyond the burnoff limit.

Models involving the synchrotron emission by secondary leptons represent an extreme realization of scenarios where the site of particle acceleration and emission are physically separated. Such scenarios do not necessary require violation of the ideal MHD conditions. If a considerable gradient of the magnetic field is present in the source, then particles accelerated in regions of weak magnetic field can travel up to regions with strong magnetic fields and eventually produce synchrotron component extending beyond the burnoff limit. Some models invoke conversion between charged and uncharged state of leading particle (e.g., via a cycle of pair production and inverse Compton scattering in the Klein-Nishina regime), which allows avoiding synchrotron losses during the propagation to a strong B-field region.

Efficiency of acceleration process influences the position of the cutoff of the synchrotron spectrum. In the case of stochastic particle acceleration, the spectrum of electrons does not stop abruptly but extends beyond E_e^{MAX} , although with a rather sharp cutoff shape, e.g., exponential or faster. Typically, the maximum of the SED, νF_ν , appears at the energy exceeding $h\nu^{\text{MAX}}$. However, for any realistic spectrum of electrons, the shift does not exceed a factor of a few. If one considers acceleration processes operating in non-ideal MHD configurations, then one may expect high acceleration efficiencies, $\eta < 1$, and the synchrotron spectrum can extend considerably above the burnoff limit. Reconnection of magnetic field lines represents a non-ideal MHD process that is believed to play important role in particle acceleration in different astrophysical sources, including pulsar wind nebulae and jet from active galactic nuclei. We note that there is a quite broad spectrum of processes that can get activated at magnetic reconnection and enhance particle acceleration. For example, this includes Fermi I acceleration in converging flows mediated by magnetic reconnection [Bosch-Ramon \(2012\)](#), transformation of turbulent cascade with an important feedback on particle acceleration [Lazarian et al. \(2020\)](#). Among other effects, the acceleration in the current sheet of X-point is of special interest ([Cerutti et al. 2013](#)). In such regions, the reconnecting magnetic field annihilate leaving guide magnetic field and unscreened electric field $\mathcal{E}_0 \simeq \beta B_0$, where $\beta \sim \mathcal{O}(1)$ is the inflow speed. Although this configuration reassembles the models with different accelerator and emitter magnetic fields discussed above, we note a principle differences between these two cases: the reconnection current sheet is not a region with an ideal MHD flow, so the burnoff limit is not applicable for that configuration.

If the particle confinement time in the current sheet is long enough to accelerate particles beyond E_e^{MAX} , then these energetic particles should produce emission that peaks above the burnoff limit once they escape into the regions with magnetic field B_0 . It may seem that scenarios involving particle acceleration in current sheets alleviate completely the constraint imposed by synchrotron cooling. However, in any realistic configuration there are still important further limitations. Firstly, to generate a synchrotron component that extends in to VHE regime the linear size of the accelerator should be sufficiently large,

$$\begin{aligned} \lambda_{\text{ACC}} &\geq 50 \beta^{-1} \left(\frac{B_{\text{cr}}}{B_0 \alpha} \right)^{3/2} \frac{e^2}{m_e c^2} \\ &\geq 2 \times 10^{17} \beta^{-1} \left(\frac{B_0}{1 \text{ mG}} \right)^{-3/2} \text{ cm}, \end{aligned} \tag{1}$$

where B_{cr} is the Schwinger critical field strength. Existence of such extended coherent reconnection site is questionable. Another important factor is the influence of the guide magnetic field, which should be present unless the reconnecting magnetic fields are perfectly antiparallel. Guide magnetic fields not only lead to synchrotron cooling, but also enhance escape of high energy particles from the current sheet. These two factors are expected to suppress significantly the efficiency of the synchrotron process in the VHE regime.

Finally, the sharp decrease at the end of the synchrotron spectrum can be altered in a medium with inhomogeneous magnetic fields. For the case of highly turbulent magnetic fields whose correlation length crossing time, λ_B/c , is small compared to the electron's inverse cyclotron frequency, $1/\omega_c = m_e c/eB_0$, the radiation proceeds in the so-called jitter regime. In this case, the peak in the radiation spectrum is shifted to higher frequencies by a factor of $c/(\omega_c \lambda_B)$ (Kelner et al. 2013). Thus, for scenarios with extremely small-scale turbulence, one can formally expect radiation in the multi-GeV or higher energies. However, the plasma physics community has been quite pessimistic concerning the condition of $\lambda_B \ll c/\omega_c$, and correspondingly considers the realization of magnetobremsstrahlung in the jitter regime as a highly unlikely process. In principle, the presence of large scale turbulence, $\lambda_B > c/\omega_c$, can also have an impact on the SED of synchrotron radiation. In particular, a broad power-law distribution of the magnetic field strength can result in a rather long power-law tail of radiation beyond $h\nu^{\text{MAX}}$ (Kelner et al. 2013). However, for more realistic magnetic field strength distributions, e.g., a Gaussian type distribution, the shift of the synchrotron peak is rather mild (Derishev & Aharonian 2019).

3. TOY MODEL: MATHEMATICAL FORMULATION

Although the postulation of magnetic field blobs inside the particle accelerator implies that we deal with a multi-zone scenario, mathematically one can describe the problem within a one-zone model. In this case, the description of the process is similar to the so-called *leaky-box approximation* which has been successfully applied to Galactic cosmic rays:

$$\frac{\partial n}{\partial t} + \frac{\partial(\dot{E}n)}{\partial E} + \frac{n}{\tau} = q(E). \quad (2)$$

Here τ is the particle – magnetic blob collision time, and \dot{E} is the energy loss rate of electrons in the main (acceleration) zone depends on particle energy and magnetic field strength given by

$$\dot{E}(E) = -\frac{E}{t_{\text{SYN}}(E, B_0)} = -\frac{\sigma_{\text{T}} B_0^2 E^2}{6\pi m_e^2 c^3}. \quad (3)$$

Within the standard treatment, these terms are responsible for the continuous and catastrophic losses of electrons, respectively. The function $q(E)$ accounts for a phenomenological description of the acceleration process. Eq. (2) is valid for particles with energy $E > E_*$; the boundary energy is obtained from the solution of the equation:

$$t_{\text{SYN}}(E_*, B_*) = t_*, \quad (4)$$

where B_* is the magnetic field and t_* is the electron confinement time in the blobs. The latter generally depends on the particle energy. See Appendix A for the justification of Eq. (2). The relevant time-scales are shown in Fig. 1. We assume that in absence of magnetic blobs the injection spectrum contains a cutoff at energy E^{MAX} which is determined from the condition $t_{\text{ACC}}(E^{\text{MAX}}) = t_{\text{SYN}}(E^{\text{MAX}}, B_0)$. We define this timescale t^{MIN} . If the collision time is long compared to the acceleration time up to energy E^{MAX} , i.e.

$$\tau > t^{\text{MIN}}, \quad (5)$$

then the impact of the magnetic blobs on the maximum energy of accelerated electrons can be ignored. Additionally, it is also helpful to define another timescale $t^{\text{MAX}} = t_{\text{SYN}}(E_*, B_0)$. The spectral shape of electrons in the cutoff region depends on the specific acceleration process. Below, we assume that $q \propto E^{-\alpha} \exp[-(E/E^{\text{MAX}})^{\beta}]$, where for simplicity, but without loss of generality, we adopt $\alpha = 2$ and $\beta = 1$.

In the fast cooling regime, when the injection and losses processes balance one another, the solution of Eq. (2) is

$$n(E, t) = -\frac{1}{\dot{E}} \int_E^{\infty} dE' q(E') \exp\left[-\frac{\tau_{\text{EFF}}(E, E')}{\tau}\right], \quad (6)$$

where the auxiliary function τ_{EFF} is

$$\tau_{\text{EFF}}(E, E') = -\int_E^{E'} \frac{dE''}{\dot{E}(E'')} = \frac{6\pi m_e^2 c^3}{(\sigma_{\text{T}} B_0^2)} \left(\frac{1}{E} - \frac{1}{E'}\right). \quad (7)$$

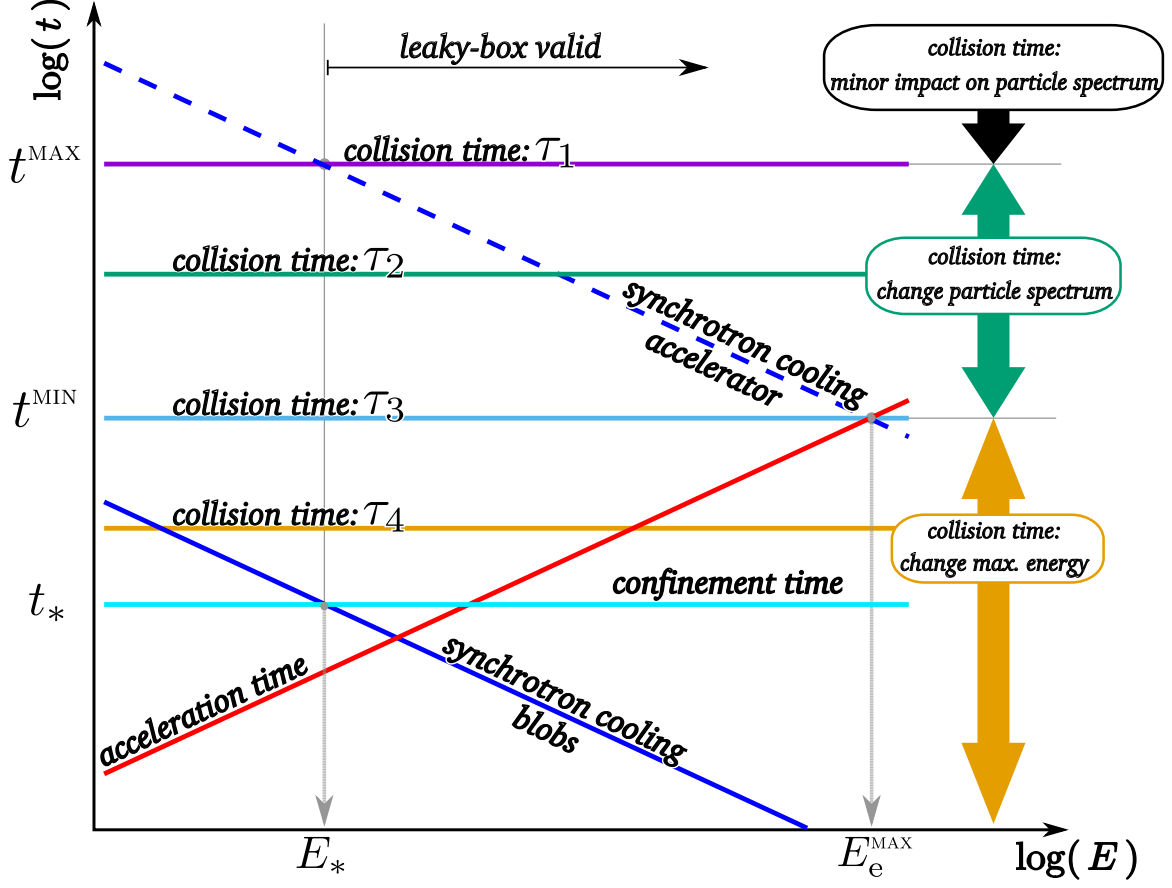


Figure 1. Characteristic time scales: the acceleration time in the main (acceleration) zone, t_{ACC} , (red line); the weak field synchrotron cooling time in the main zone, $t_{\text{SYN}}(E, B_0)$, (blue dashed line); the strong field synchrotron cooling time in the blobs, $t_{\text{SYN}}(E, B_*)$, (blue solid line); the confinement time of the electron in the blobs, t_* , (cyan line). Four characteristic collision times are considered: the purple curve for $\tau = t^{\text{MAX}}$, the green curve for $\tau = \sqrt{t^{\text{MIN}} t^{\text{MAX}}}$, the light blue curve for $\tau = t^{\text{MIN}}$, and the orange curve for $\tau < t^{\text{MIN}}$. Note, the timescales t^{MIN} and t^{MAX} are defined as $t_{\text{SYN}}(E^{\text{MAX}}, B_0)$ and $t_{\text{SYN}}(E_*, B_0)$, respectively.

Two distinct components of synchrotron emission are produced in this scenario. In the main zone, the synchrotron radiation produced by electrons with an energy distribution given by Eq. (6), takes a spectral shape of the form

$$L_{\nu,0} = \int P_{\nu}(B_0, E)n(E)dE, \quad (8)$$

where P_{ν} is the power per unit frequency emitted by an electron with energy E . The electrons that enter the blob, with its much stronger magnetic field, quickly emit their energy at a rate $1/\tau$. The time-averaged energy spectrum of their synchrotron radiation produced in the magnetic blobs is

$$L_{\nu,*} = \frac{1}{\tau} \int \left[\int_0^{t_*} dt P_{\nu}(B_*, \tilde{E}(t, B_*)) \right] n(E)dE, \quad (9)$$

where $\tilde{E}(t, B) = E/(1 + t/t_{\text{SYN}}(E, B))$ (see Appendix B).

As demonstrated in Fig. 1, for the condition given by Eq. (5) two different scenarios exist: $\tau \geq t^{\text{MAX}}$ and $t^{\text{MIN}} < \tau < t^{\text{MAX}}$. In the first of these regimes, the presence of magnetic field blobs has only a minor impact on the particle spectrum, i.e., $\tau \gg \tau_{\text{EFF}}$. In the second regime the particle spectrum is deformed by interactions with the magnetic blobs, although the maximum energy of the particle spectrum remains unaffected.

In Figs. 2 and 3, we show the corresponding SEDs produced in four different collision timescale scenarios illustrated in Fig. 1. In these figures two different strengths of the blob magnetic field, $B_* = 10^2 B_0$ and $B_* = 10^3 B_0$, are considered.

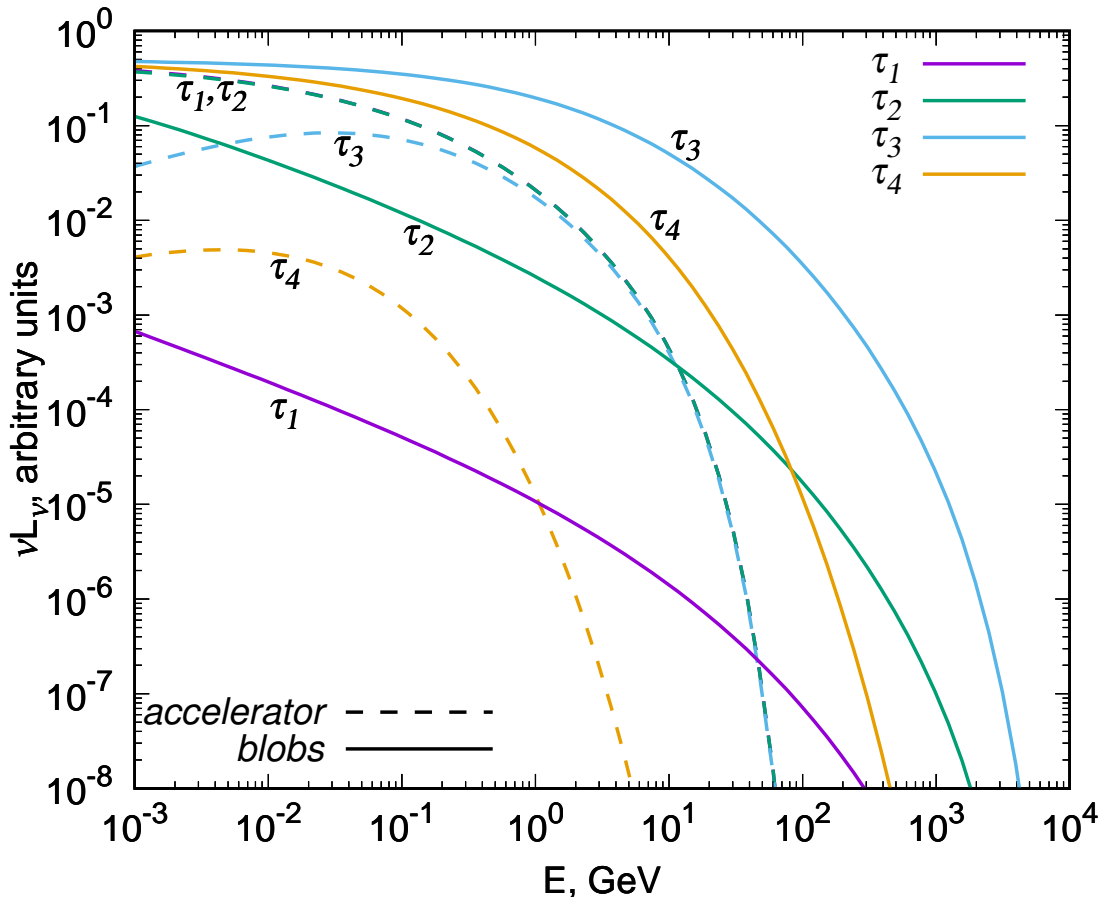


Figure 2. Characteristic spectral energy distributions for four example cases considered in Fig. 1 (the same line colors for the cases considered in Fig. 1 are used here also). The dashed lines indicate the emission from particles in the accelerator magnetic field ($B_0 = 0.1$ G), and the solid lines indicate the emission from particles in the blobs of size $R = 3 \times 10^{13}$ cm having magnetic field of $B_* = 10^2 B_0$.

These results show that for particular values of the collision time considered, the synchrotron radiation produced in the blobs indeed extends up to a factor B_*/B_0 beyond the limit $h\nu^{\text{MAX}}$. However, for the case of $\tau > t^{\text{MAX}}$, the overall luminosity of this high energy emitted component is significantly less than that produced in the main zone. Only for the case of small collision timescales, $\tau < t^{\text{MAX}}$, is the SED dominated by the emission produced in the blobs. The dashed curves in these figures correspond to the emission in the accelerator's magnetic field B_0 and the solid curves correspond to the emission in the blob's magnetic field B_* . If particles enter the strong magnetic field region during the acceleration process then the maximum attainable energy can be significantly affected, decreasing the energy of the SED maximum formed in the blobs (the case of τ_4 in Figs. 2 and 3).

4. PHYSICAL JUSTIFICATION OF THE TOY MODEL

The mathematical model introduced in Sec. 3 formally depends on a single parameter, τ . However, there are two hidden parameters, t_* and B_* , which determine the energy range where the leaky box approximation used is actually valid. Furthermore, the main zone is characterized by two parameters: the size, R and the magnetic field, B_0 . The question remains whether there exists a physically meaningful combination of these parameters which would allow the realization of the radiation scenario illustrated in Fig. 2.

For the sake of simplicity, we assume that there exist \mathcal{N} identical small scale large field blobs of size r_* . The interaction time of electrons with these blobs lasts a minimum duration of $t_* \simeq r_*/c$. This interaction time can be significantly longer if the electron is magnetically confined within the blob. To avoid this complication, we focus on sufficiently high electron energies (above E_*) such that the electron life-time is shorter than their minimal confinement time in the blobs $\sim r_*/c$.

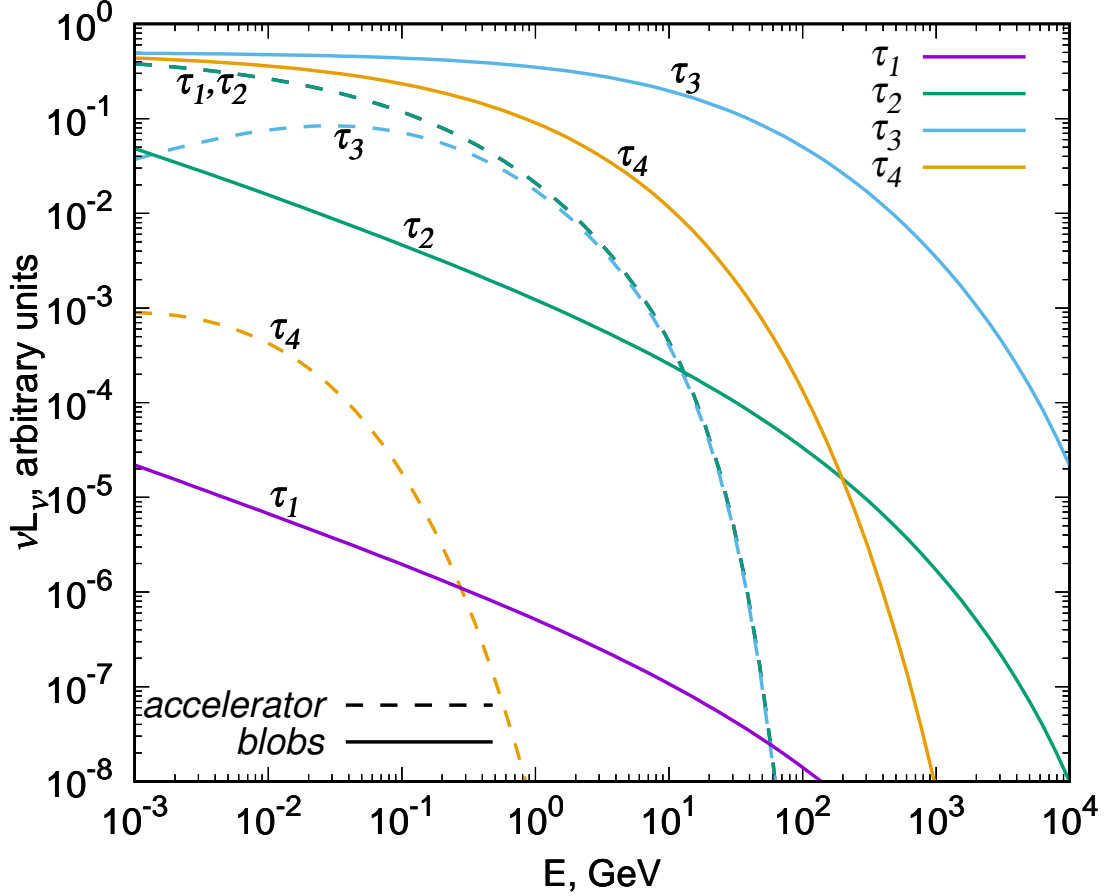


Figure 3. The same as Fig. 2 but for $B_* = 10^3 B_0$.

For the strong field of the blobs, the geometrical size of the blob dictates the collision time of the electrons with them,

$$\tau \simeq \frac{R^3}{\mathcal{N}\pi r_*^2 c}, \quad (10)$$

where we used R^3 for the volume of the main zone. On the other hand, the magnetic field strength of the blob determines the electron energy above which the leaky-box treatment remains valid:

$$E_* = \frac{6\pi m_e^2 c^4}{\sigma_T r_* B_*^2}. \quad (11)$$

The scenario introduced in Sec. 3 is realized when the following three conditions are satisfied: (i) $t^{\text{MIN}} < \tau < t^{\text{MAX}}$, (ii) $E_* \ll E^{\text{MAX}}$, and (iii) $B_* \gg B_0$. The former condition determines the range for \mathcal{N} , and can be fulfilled without interference with the two other conditions. We therefore need to check just one condition, $E_* \ll E^{\text{MAX}}$, in the limit $B_* \gg B_0$:

$$r_* \gg \frac{B_0^2 E^{\text{MAX}} \eta}{B_*^2 e B_0}. \quad (12)$$

From the application of the maximum energy condition for a source (“Hillas criterion”) $E^{\text{MAX}}/(eB_0) < R$, it follows that there should exist a range of r_* such that $E_* \ll E^{\text{MAX}}$ and $r_* \ll R$. However, this requires a large ratio of magnetic fields: $B_* \gg B_0$.

Let us estimate the fraction of the magnetic energy in the blobs required for strong boosting of the radiation energy. It is determined by the condition $\tau \ll t^{\text{MAX}}$:

$$\frac{\delta w_B}{w_B} = \frac{4\pi\mathcal{N}}{3} \frac{r_*^3 B_*^2}{R^3 B_0^2} = \frac{4}{3} \frac{t^{\text{MAX}}}{\tau} \geq 1. \quad (13)$$

This implies that significant transformation of the synchrotron spectrum beyond $h\nu^{\text{MAX}}$ is possible when the magnetic energy in the small blobs dominates over the energy in the main zone magnetic field. Note that this condition can be realized only in weakly magnetized environments, where the energy contained in the particles can provide an ample source for the formation of strong magnetic fluctuations (blobs). If the particle internal energy is transferred to the magnetic form in blobs, then the total pressure in the blobs should not exceed the external pressure, preventing such regions of strong magnetic field from instantly expanding.

We note that such conditions with weakly magnetized plasma are expected in several important gamma-ray sources. For example, while pulsar winds are believed to be weakly magnetized close to the termination shock, the overall conditions in pulsar wind nebulae favor equipartition of gas and magnetic pressure. Thus, initially weak magnetic field gets significantly amplified in the nebula. Another example could be gamma-ray burst afterglow emission. According to the standard framework, the afterglow emission is generated by particles that are accelerated at the GRB forward shock that propagates through the circumburst medium. If the circumburst medium magnetic field is $\sim 10\mu\text{G}$, then the initial plasma magnetization is extremely small, say 10^{-10} . The amplification of such a weak magnetic field to some ‘‘equipartition’’ strength may create conditions favorable for the formation of compact magnetic blobs.

5. MAGNETIC MIRRORING

Another important aspect is the ability of particles to enter the regions of strong magnetic field. If the change of magnetic field is small, then particles moves in a way that the adiabatic invariant p_{\perp}^2/B is approximately conserved. In this case the conservation of energy prevents particle penetration into a region with a significantly stronger magnetic field. To take account of this effect, which is known as magnetic mirroring, and allow particle penetration from a region with magnetic field B_0 , the following condition should be fulfilled:

$$T \frac{dB}{dt} \gtrsim B_0, \quad (14)$$

where $T \sim 2\pi E/eB_0c$ and $dB/dt \sim cB_*/r_*$ are the particle giro-rotation period and effective rate of the magnetic field change. Solving Eq. 15 for particle energy, we obtain the minimum energy of particles that can penetrate into the blobs:

$$E^{\text{MIN}} = \frac{1}{2\pi} \frac{B_0}{B_*} r_* e B_0. \quad (15)$$

The realization of the discussed scenario requires that $E^{\text{MIN}} \ll E^{\text{MAX}}$, which can be written as a condition on the blob size:

$$r_* \ll \frac{2\pi B_* E^{\text{MAX}}}{B_0 e B_0}. \quad (16)$$

For $B_* \gg B_0$, Eqs. (12) and (16) can be simultaneously fulfilled.

Equations (16) and (20) show that for the relevant range of magnetic blob sizes, the magnetic mirroring effect should not prevent penetration of particle into the regions of strong magnetic field. However, even if a particle penetrates to the blob, it doesn’t necessarily mean that it could interact with the strongest field. For any realistic configuration of the field, there should exist a gradual increase from the main-zone field strength, B_0 , to the blob field, B_* . Motion of a particle in this boundary layer might be very complicated. Although the adiabatic invariant should not be conserved at a strong gradient of magnetic field, we may use it to estimate how deep a particle can penetrate into the blob. We assume that the strongest magnetic field strength, $B(E)$, a particle with energy E can reach, is determined by a relation similar to Eq. (15):

$$\frac{2\pi E}{eB(E)c} \frac{B_*c}{r_*} \simeq B(E). \quad (17)$$

We note that this condition corresponds to the strongest magnetic mirroring. The level of the real effect might be significantly smaller. For example, observations of gamma-ray emission from the Sun (Linden et al. 2018) suggest that magnetic mirroring is not as efficient for reflecting high-energy particles as it was naively expected (Seckel et al. 1991).

Solving Eq. (17) for $B(E)$, we obtain:

$$B(E) \simeq \sqrt{\frac{2\pi E B_*}{e r_*}}. \quad (18)$$

In addition one should take into account that the minimum and maximum magnetic field strength are B_0 and B_* , respectively.

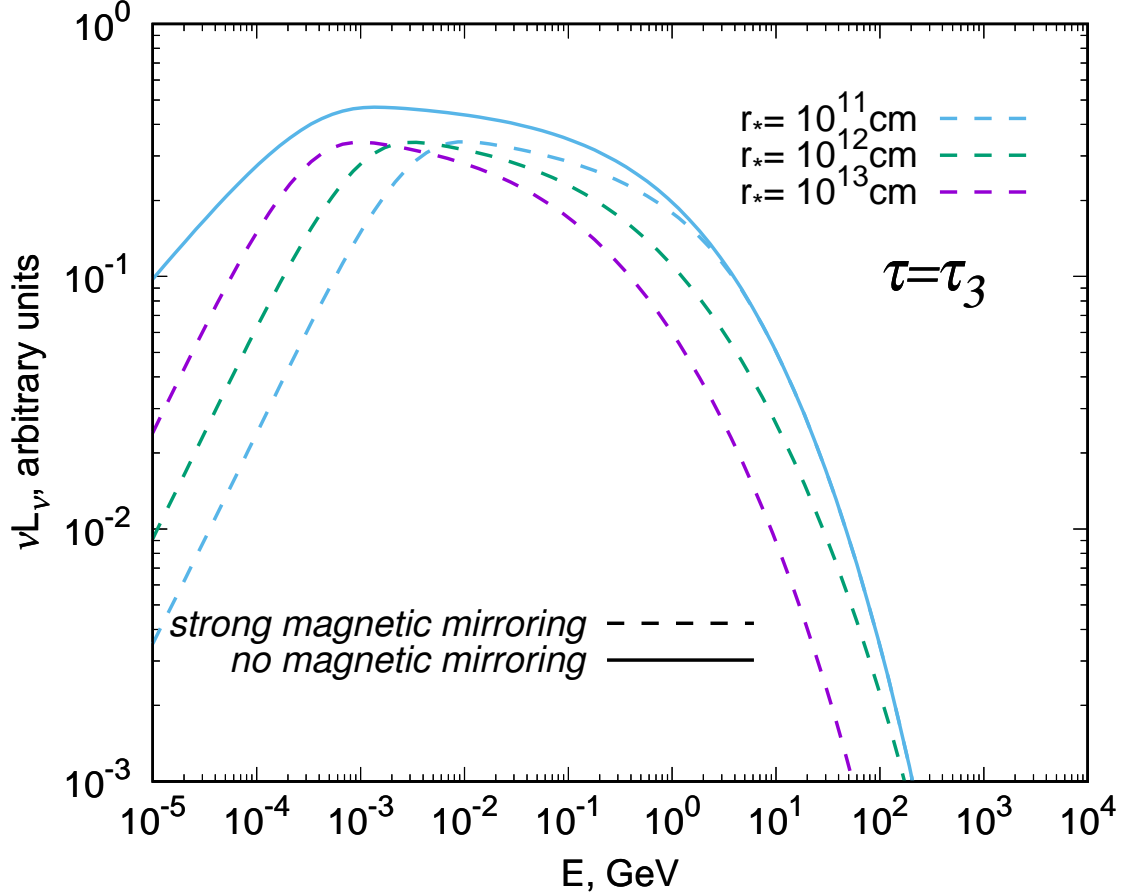


Figure 4. Characteristic spectral energy distributions from magnetized blobs showing the impact of strong magnetic mirroring for $\tau = \tau_3$ and three different blob sizes: $r_* = 10^{13}$ cm, $r_* = 10^{12}$ cm, and $r_* = 10^{11}$ cm. The rest of the parameters are the same as in Fig. 2.

To estimate the strongest possible impact of the magnetic mirroring, we compute the spectrum from the blob using the energy dependent magnetic field strength, Eq. (18):

$$L_{\nu,*}^{\text{mir}} = \frac{1}{\tau} \int \left[\int_0^{t_*} dt P_\nu(B(E), \tilde{E}(t, B(E))) \right] n(E) dE \quad (19)$$

(compare to Eq. (9)). In Figs. 4 and 5 we show the corresponding SEDs for three different blob sizes: $r_* = 10^{13}$ cm, $r_* = 10^{12}$ cm, and $r_* = 10^{11}$ cm. As can be seen, in the case of strong magnetic mirroring, the spectra can become significantly suppressed at low energies. This is caused by significant reflection of low-energy electrons. Higher energy particles may have difficulties in reaching the strongest magnetic field, which results in spectrum suppression for large blobs, $r_* \geq 10^{12}$ cm.

6. DISCUSSION

The synchrotron radiation of relativistic electrons is a unique process that proceeds with high efficiency in a wide variety of astrophysical environments, and spans a broad energy range from radio up to gamma-rays. The typical short time-scales characterizing the synchrotron cooling of electrons make this process the dominant radiation channel not only at radio wavelengths but also in the relatively low (Sub-GeV) energy gamma-ray band. This is the case, for example, of gamma-ray bursts (Ajello et al. 2018) or the so-called Crab flares (Bühler & Blandford 2014). The characteristic spectral and temporal features of this mechanism seem very attractive for interpretation of the fast and energetic phenomena in the very high energy gamma-ray band as well. One may recall, for example, the ultrafast

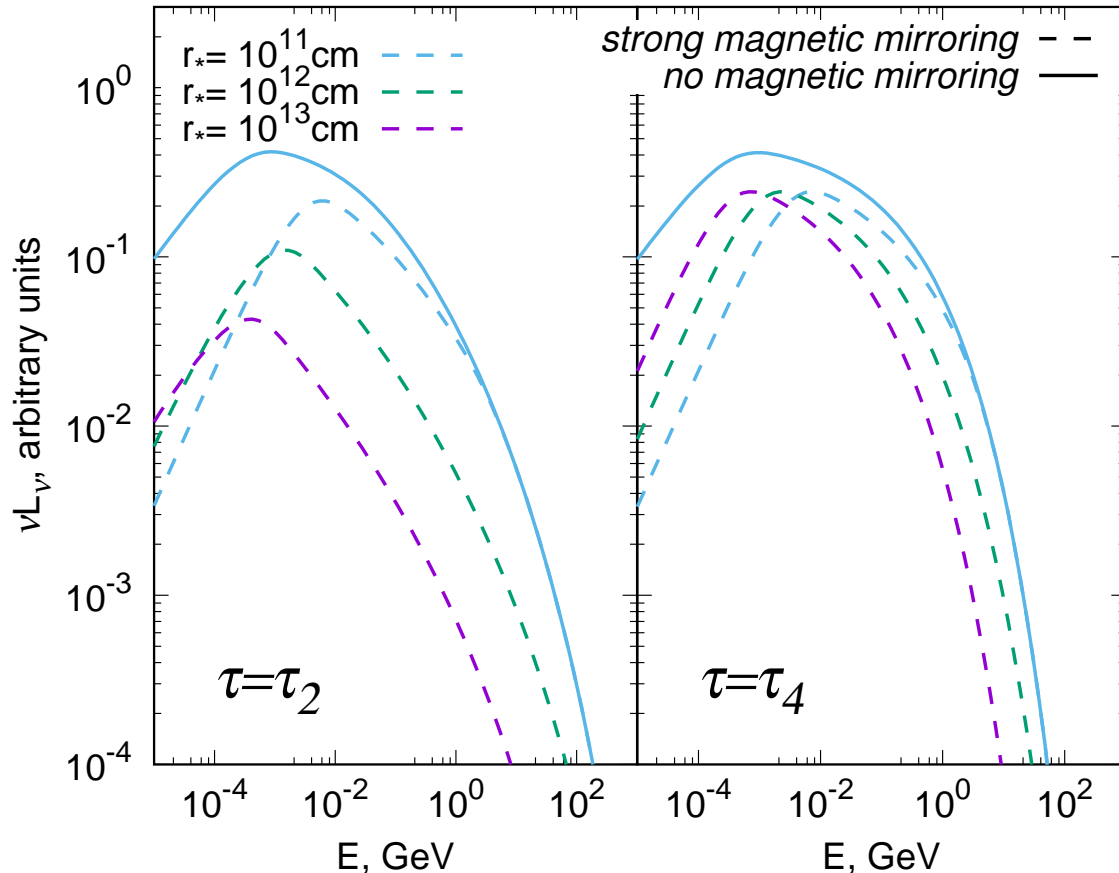


Figure 5. The same as Fig. 4 but for $\tau = \tau_2$ (left panel) and $\tau = \tau_4$ (right panel).

VHE gamma-ray flares of blazars (Aharonian et al. 2007; Aleksić et al. 2014) or extension of the gamma-ray spectra of late afterglows of GRBs (Abdalla et al. 2019). However, the self-regulated cutoff in the synchrotron spectrum at ≤ 100 MeV has been thought to limit the applicability of the process for energies well above 100 MeV (in the frame of the source).

Synchrotron radiation can be significantly boosted in sources where the emission region moves relativistically, $h\nu^{\text{MAX}} \simeq 70 \mathcal{D}$ MeV. The Doppler boosting of the maximum of synchrotron radiation can be naturally realized in relativistic outflows like the jets of active galactic nuclei (AGN) and gamma-ray bursts (GRBs). Typically, in the AGN and late GRB afterglows, the jet’s Doppler factors do not exceed 100. Thus the Doppler boosting alone cannot shift the synchrotron radiation to very-high energies, especially given that in realistic conditions, e.g. with the inclusion of the presence of dissipative factors like adiabatic losses or plasma instabilities, the η -parameter may significantly exceed 1. The consideration of physically realistic values for η , therefore, exacerbates further the problem of accounting for emission at the $h\nu^{\text{MAX}}$ scale as being synchrotron in origin.

In this paper, we propose a scenario for the formation of synchrotron radiation in compact magnetic blobs located inside the particle accelerator. The blobs do not participate in the acceleration process but serve as passive targets where the highest energy electrons accelerated in the main zone, are instantly cooled via synchrotron losses, whose spectrum is effectively extended up to the VHE band. We have developed a simple mathematical formalism based on a “leaky box” approach, for calculations of synchrotron radiation emerging from such systems. The results of numerical calculations confirm the qualitative estimates. They demonstrate that the synchrotron radiation of such systems can be effectively released in the very-high-energy regime provided that the magnetic field in the blobs exceeds two or three orders of magnitude the magnetic field in the accelerator zone. Although the compact magnetic condensations occupy a rather small volume inside the accelerator, the total magnetic energy in these blobs should significantly exceed the electromagnetic energy contained in the acceleration zone. Remarkably, the MHD studies of magnetic amplification by

turbulent dynamo (Zhang et al. 2009) in relativistic outflows may result in such systems where the magnetic energy is predominantly contained in compact clumps. Moreover, this amplification of small scale fields may be a general effect (Kazantsev 1968).

As shown in Sec. 4, the hierarchy of the characteristic timescales determining the feasibility of the scenario is such that the extension of the blob synchrotron component to the VHE regime is possible. Let us here outline some criteria for that regime. The toy model from Sec. 4 contains six parameters: R , B_0 , η , r_* , \mathcal{N} , and B_* . It is convenient to replace parameter \mathcal{N} with *filling factor*, i.e., $\mathcal{F} = 4\pi/3\mathcal{N}(r_*/R)^3 = 4/3r_*/(\tau c)$, as it allows us to eliminate the dependences on the size of the system, R . Thus, the radiation regime depends on only five parameters.

The extension of the synchrotron component allows one to define the strength of the blob magnetic field: $B_* \sim 10^3 B_0 \eta$. This component has a significant luminosity if $\tau \simeq t^{\text{MIN}}$, which translates into condition $\mathcal{F} \sim 4/3r_*/(t^{\text{MIN}}c)$. These two conditions further reduce the number of free parameters. Finally, two conditions, $\mathcal{F} \ll 1$ and Eq. (12), define the allowed range for r_* :

$$\frac{3}{4} \frac{\eta E_e^{\text{MAX}}}{e B_0} \gg r_* \gg 10^{-6} \frac{E_e^{\text{MAX}}}{e B_0 \eta}, \quad (20)$$

where E_e^{MAX} depends on B_0 and η :

$$E_e^{\text{MAX}} = \sqrt{\frac{6\pi e m_e^2 c^4}{\sigma_T \eta B_0}} = 2 \left(\frac{\eta B_0}{1 \text{ mG}} \right)^{-1/2} \text{ PeV}. \quad (21)$$

Normalizing the magnetic field to 1mG, one obtains

$$\frac{3}{4} \eta^{1/2} \left(\frac{B_0}{1 \text{ mG}} \right)^{-3/2} \gg \frac{r_*}{6 \times 10^{15} \text{ cm}} \gg 10^{-6} \eta^{-3/2} \left(\frac{B_0}{1 \text{ mG}} \right)^{-3/2}. \quad (22)$$

This multi-decade range shows that the requirements for the discussed scenario can be relatively easily met in astrophysical sources. We note here that Eq. 16 provides a weaker constraint on the blob size compared to Eq. (20). Furthermore, even for the extreme case of effective magnetic mirroring, this scenario can still be realized provided that the blobs have a sufficiently small size:

$$10^{-2} \eta^{-3/2} \left(\frac{B_0}{1 \text{ mG}} \right)^{-3/2} \gtrsim \frac{r_*}{6 \times 10^{15} \text{ cm}} \gg 10^{-6} \eta^{-3/2} \left(\frac{B_0}{1 \text{ mG}} \right)^{-3/2}. \quad (23)$$

ACKNOWLEDGMENTS

We thank anonymous referee for useful comments that helped us to improve the manuscript. DK acknowledges support by JSPS KAKENHI Grant Numbers 18H03722, 18H05463, and 20H00153.

APPENDIX

A. LEAKY-BOX APPROXIMATION

Magnetic field fluctuations play a key role in both sink and source terms in the standard injection-cooling equation:

$$\frac{\partial n}{\partial t} + \frac{\partial(\dot{E}n)}{\partial E} + \frac{n}{\tau} - \frac{n(\tilde{E})}{\tau} = q(E), \quad (A1)$$

where $q(E)$ is the injection term, $n = dN/dE$ is energy-distribution function, \dot{E} is energy losses in the main zone magnetic field, τ is the particle – fluctuation collision time, $\tilde{E}(E)$ is the particle energy that cools down to E while interacting with the fluctuation. While the particle is interacting with the fluctuation, it loses energy via synchrotron emission in the strong magnetic field of strength B_* . If the confinement time is t_* , then the initial and final particle energies (\tilde{E} and E , respectively) are related as

$$\frac{E}{E_*} = \frac{\tilde{E}}{E_*} \frac{1}{1 + \frac{\tilde{E}}{E_*}}, \quad (A2)$$

where $t_{\text{SYN}}(E, B_*) (\propto E^{-1} B_*^{-2})$ is the synchrotron cooling time in the magnetic field of strength B_* and E_* is the solution of equation $t_* = t_{\text{SYN}}(E_*, B_*)$. According to Eq. (A2), for the energy range $E > E_*$, there are no particles that cool down to E and Eq. (A1) takes a simple form

$$\frac{\partial n}{\partial t} + \frac{\partial(\dot{E}n)}{\partial E} + \frac{n}{\tau} = q(E), \quad (\text{A3})$$

which is identical to the equation for transport of cosmic ray under the leaky-box approximation. It allows a well-known analytical solution (Syrovatskii 1959):

$$n(E, t) = -\frac{1}{E} \int_E^{E_{\text{EFF}}} dE' q(E') \exp\left[-\frac{\tau_{\text{EFF}}(E, E')}{\tau}\right]. \quad (\text{A4})$$

Here the auxiliary parameters, E_{EFF} and τ_{EFF} , are

$$t = -\int_E^{E_{\text{EFF}}} \frac{dE'}{\dot{E}(E')} \quad (\text{A5})$$

and

$$\tau_{\text{EFF}}(E, E') = -\int_E^{E'} \frac{dE''}{\dot{E}(E'')}. \quad (\text{A6})$$

Since the dominant cooling mechanism is synchrotron losses the above integral can be derived analytically.

B. APPROXIMATED EXPRESSION FOR THE SYNCHROTRON SPECTRUM

The total emission of a particle that enters a high magnetic field region needs to be computed accounting for the change of the particle energy. To be consistent with the standard textbooks, we operate with the total emitted energy per frequency:

$$E_\nu = \int_0^{t_*} P_\nu(E(t, B)) dt = \frac{\sqrt{3}e^3 B}{m_e c^2} \int_0^{t_*} F_\nu(x(t, B)) dt, \quad (\text{B1})$$

where

$$F(x) = x \int_x^\infty K_{5/3}(\xi) d\xi \quad (\text{B2})$$

and

$$x(t, B) = \frac{4\pi\nu m_e^3 c^5}{3E_0^2 e B} u^2 = \nu_0 u^2(t, B) \quad (\text{B3})$$

(here $u(t, B) = E_0/E(t, B)$ and the above equation defines ν_0). In Eq. (B1) the particle energy, $E(t)$, depends on the initial energy, E_0 , as

$$E(t, B) = \frac{E_0}{1 + t/t_{\text{SYN}}(E_0, B)} \quad (\text{B4})$$

and

$$dt = t_{\text{SYN}}(E_0, B) du. \quad (\text{B5})$$

Although, formally, Eq. (B1) is a four-parameter function, it is clear that

$$E_\nu(E_0, B, t_*) = E_\nu(E_0, B, \infty) - E_\nu(E(t_*, B), B, \infty), \quad (\text{B6})$$

which allows one to reduce the dependence on t_* , and in what follows we consider Eq. (B1) in the limit $t_* \rightarrow \infty$.

Combining the above equations, one obtains

$$\begin{aligned} E_\nu &= \frac{\sqrt{3}e^3 B t_{\text{SYN}}(E_0, B)}{m_e c^2} \int_1^\infty du \nu_0 u^2 \int_{\nu_0 u^2}^\infty d\xi K_{5/3}(\xi) \\ &= \frac{\sqrt{3}e^3 B_* t_{\text{SYN}}(E_0, B)}{m_e c^2} G(\nu_0). \end{aligned} \quad (\text{B7})$$

Changing the integral order allows one to derive one integral in the auxiliary function analytically:

$$G(\nu_0) = \frac{\nu_0}{3} \int_{\nu_0}^\infty d\xi K_{5/3}(\xi) \left(\left(\frac{\xi}{\nu_0} \right)^{3/2} - 1 \right). \quad (\text{B8})$$

Using the approach introduced in [Khanguyan et al. \(2014\)](#), we approximate Eq. (B8) with a simple analytic function:

$$G(x) \simeq \tilde{G}(x) = \frac{1.04e^{-x}}{\sqrt{x}} \left(\frac{1 + 0.464x}{1 + 0.771x} \right) g(x), \quad (\text{B9})$$

where

$$g(x) = \left[1 + \frac{ax^\alpha}{1 + bx^\beta} \right]^{-1} \quad (\text{B10})$$

for $a = 0.186$, $\alpha = 0.57$, $b = 1.75$, and $\beta = 1.49$. This approximation has exact asymptotical behavior for $x \rightarrow 0$ and ∞ . In the entire range it provides an accuracy of $\simeq 0.2\%$ as shown in Fig. 6.

REFERENCES

- Abdalla, H., et al. 2019, *Nature*, 575, 464, doi: [10.1038/s41586-019-1743-9](https://doi.org/10.1038/s41586-019-1743-9)
- Aharonian, F., et al. 2007, *ApJL*, 664, L71, doi: [10.1086/520635](https://doi.org/10.1086/520635)
- Aharonian, F. A. 2000, *NewA*, 5, 377, doi: [10.1016/S1384-1076\(00\)00039-7](https://doi.org/10.1016/S1384-1076(00)00039-7)
- Ajello, M., et al. 2018, *ApJ*, 863, 138, doi: [10.3847/1538-4357/aad000](https://doi.org/10.3847/1538-4357/aad000)
- Aleksić, J., et al. 2014, *Science*, 346, 1080, doi: [10.1126/science.1256183](https://doi.org/10.1126/science.1256183)
- Bosch-Ramon, V. 2012, *A&A*, 542, A125, doi: [10.1051/0004-6361/201219231](https://doi.org/10.1051/0004-6361/201219231)
- Bühler, R., & Blandford, R. 2014, *Reports on Progress in Physics*, 77, 066901, doi: [10.1088/0034-4885/77/6/066901](https://doi.org/10.1088/0034-4885/77/6/066901)
- Cerutti, B., Werner, G. R., Uzdensky, D. A., & Begelman, M. C. 2013, *ApJ*, 770, 147, doi: [10.1088/0004-637X/770/2/147](https://doi.org/10.1088/0004-637X/770/2/147)
- de Jager, O. C., Harding, A. K., Michelson, P. F., et al. 1996, *ApJ*, 457, 253, doi: [10.1086/176726](https://doi.org/10.1086/176726)
- Derishev, E., & Aharonian, F. 2019, *ApJ*, 887, 181, doi: [10.3847/1538-4357/ab536a](https://doi.org/10.3847/1538-4357/ab536a)
- Guilbert, P. W., Fabian, A. C., & Rees, M. J. 1983, *MNRAS*, 205, 593, doi: [10.1093/mnras/205.3.593](https://doi.org/10.1093/mnras/205.3.593)
- Kazantsev, A. P. 1968, *Soviet Journal of Experimental and Theoretical Physics*, 26, 1031
- Kelner, S. R., Aharonian, F. A., & Khanguyan, D. 2013, *ApJ*, 774, 61, doi: [10.1088/0004-637X/774/1/61](https://doi.org/10.1088/0004-637X/774/1/61)
- Khanguyan, D., Aharonian, F. A., & Kelner, S. R. 2014, *ApJ*, 783, 100, doi: [10.1088/0004-637X/783/2/100](https://doi.org/10.1088/0004-637X/783/2/100)
- Lazarian, A., Eyink, G. L., Jafari, A., et al. 2020, *Physics of Plasmas*, 27, 012305, doi: [10.1063/1.5110603](https://doi.org/10.1063/1.5110603)
- Linden, T., Zhou, B., Beacom, J. F., et al. 2018, *PhRvL*, 121, 131103, doi: [10.1103/PhysRevLett.121.131103](https://doi.org/10.1103/PhysRevLett.121.131103)
- Seckel, D., Stanev, T., & Gaisser, T. K. 1991, *ApJ*, 382, 652, doi: [10.1086/170753](https://doi.org/10.1086/170753)
- Syrovatskii, S. I. 1959, *Soviet Ast.*, 3, 22
- Zhang, W., MacFadyen, A., & Wang, P. 2009, *ApJL*, 692, L40, doi: [10.1088/0004-637X/692/1/L40](https://doi.org/10.1088/0004-637X/692/1/L40)

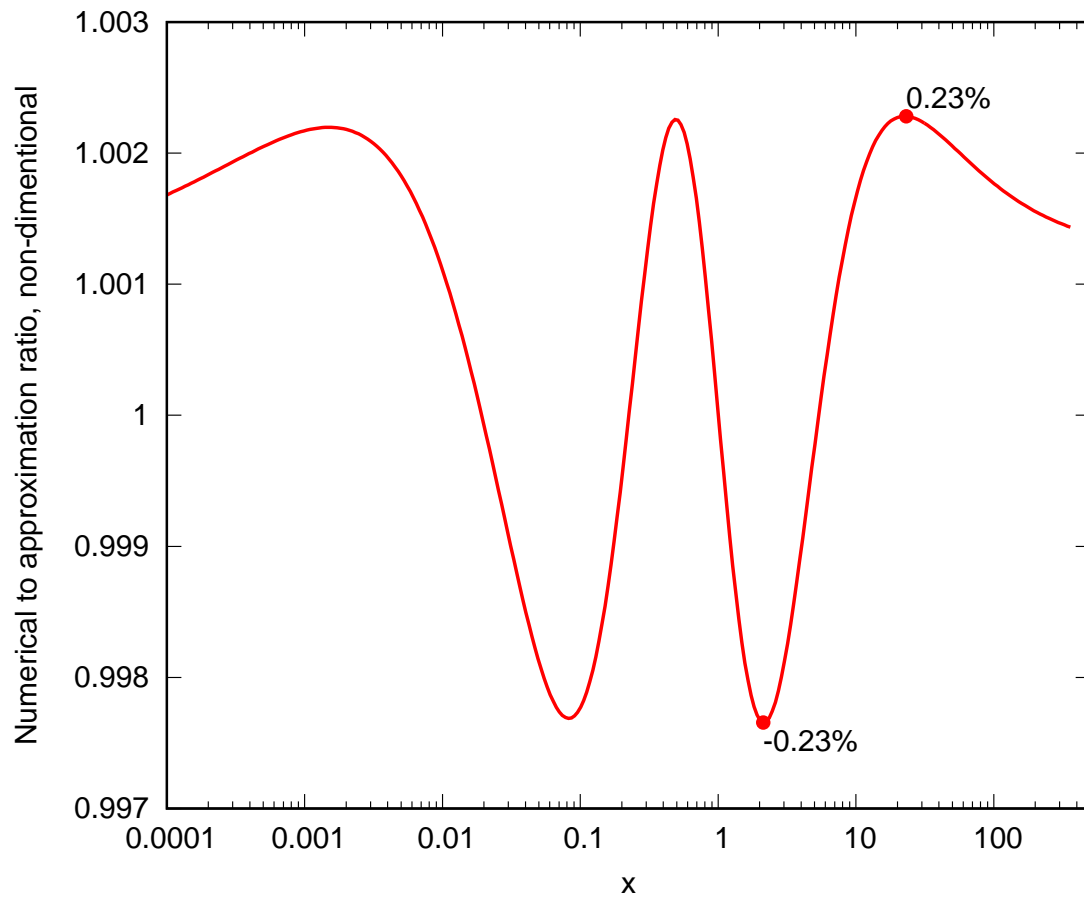


Figure 6. Ratio of the exact and approximate function that describe the synchrotron spectrum accounting for change of the particle energy.

This figure "SED.jpg" is available in "jpg" format from:

<http://arxiv.org/ps/2003.00927v2>

This figure "SED_mir.jpg" is available in "jpg" format from:

<http://arxiv.org/ps/2003.00927v2>

This figure "SED_v2.jpg" is available in "jpg" format from:

<http://arxiv.org/ps/2003.00927v2>

This figure "VHE_synchrotron_timescales_v5a.jpg" is available in "jpg" format from

<http://arxiv.org/ps/2003.00927v2>

This figure "SED_mir_tau_24.jpg" is available in "jpg" format from:

<http://arxiv.org/ps/2003.00927v2>

This figure "approximation.jpg" is available in "jpg" format from:

<http://arxiv.org/ps/2003.00927v2>